Continuous Grasping Force Estimation With Surface EMG Based on Huxley-Type Musculoskeletal Model

Xiaolei Xu, Hua Deng, *Member, IEEE*, Yi Zhang, and Jingwei Chen

***Abstract*— Continuous grasping force estimation based on electromyography (EMG) signals, is very useful in practical applications including prosthetic control and human force observation. However, implementing the practical grasping force estimation usually considers a trade-off between the computational precision and resources. Specifically, the estimation based on the Huxley-type muscle model reaches detailed approximation of physiological process at a cost of larger computational resources for solving nonlinear partial differential equations while the counterpart with a traditional Hill-type muscle model. In this article, we achieve the grasping force estimation based on a reduced Huxley-type musculoskeletal model with high accuracy yet low time delay. Leveraging on a balanced truncation method, we further reduce the dimensionality of the spectral method solution in the Huxley-type musculoskeletal model for the model simplification. In addition, we introduce the Kalman filter method to process the EMG signals obtained by an armband, yielding better real-time performances and accuracy compared to the signal treatment using the traditional EMG filter method. Moreover, we also implement an effective identification of the model parameters using a particle swarm method. Finally, we trained the model on the first day and made grasping force estimation experiments involved with three participants over the course of a month. We envision that this effective and practical method would further improve the practical applications in the field of grasping force estimation.**

***Index Terms*— Force estimation, Huxley model, surface EMG, spectral method, parameter identify, EMG filter.**

I. Introduction

AS AN easily measured bioelectric signal, the upper limb myoelectric signal has a wide range of applications in the field of medical treatment and rehabilitation [1]. This signal can control the contraction of skeletal muscles, which is observed in the form of electromyographic signals, to achieve a firm grip on an object [2]. The research on the grasping force estimation can be used to explore the principles of upper limb muscle movement, used as a control signal to achieve a variety of grasping actions of a manipulator [3], [4], and combined with feedback technology to achieve closed-loop control of grasping [5], [6]. In some studies, electromyography (EMG) signals are decoded as control signals based on classification algorithms or mathematical fitting methods, which can decode multiple grasping modes but cannot efficiently and accurately decode the grasping force [7], [8], [9], [10].

To decode EMG signal efficiently and accurately, many researchers have proposed a wide variety of force estimate methods based on the relationship between EMG signals and skeletal muscle mechanics. Engeberg [11] proposed a proportional control method which is robust as well as facile in the practical application such as the commercial prostheses but suffers from the average squared relative error of the grip and average failure rate up to 28% and 40%, respectively. Different from the inaccurate linear prediction model, nonlinear regression methods can be used estimate the parameters and predict the grasping force, which improved the percentage variance accounted for (VAF) up to 86% during gradual dynamic contraction task [12]. Furthermore, using machine learning methods can better fit the relationship between EMG signals and skeletal muscle force. Ma et al. [13] applied the convolutional neural network (CNN) to establish the relationship between the surface electromyography (sEMG) signals and forces. This method could obtain no more than five force levels proportion to the maximum voluntary contraction (MVC) after training with the correlation coefficient (CC) value of 93.14% under the five-finger pinch grasping action. As the difference between two adjacent force levels is large, the force estimation is imprecise for applications. Fang et al. [14] proposed an attribute-driven granular model (AGrM) under a machine-learning scheme to obtain more force level in different pinch-types without continuous force estimation. To realize continuous force estimation and further improve the accuracy, support vector regression (SVR) and multi-modal feature combination is implemented by Mao et al. [15] to estimates continuous grip force and further improve the cc value of continuous grip force estimation up to 95.32±1.35%. However, these methods lack an explanation of the muscle's biological mechanism and require a large amount of high-quality training data which result in a long training time and the potential overfitting.

To overcome these problems, Hill-type muscle models are used and some characteristics of biological muscle can

Manuscript received 10 March 2022; revised 23 June 2022 and 22 September 2022; accepted 11 October 2022. Date of publication 14 October 2022; date of current version 31 January 2023. This work was supported in part by the National Natural Science Foundation of China under Grant 52275297; in part by the National Key Research and Development Program of China under Grant 2018YFB1307203; in part by the Key Project of Hunan Health Commission under Grant 20200519; and in part by the Project of State Key Laboratory of High Performance Complex Manufacturing, Central South University, under Grant ZZYJKT2021-17. *(Corresponding author: Yi Zhang.)*

Xiaolei Xu and Jingwei Chen are with the School of Mechanical and Electrical Engineering, Central South University, Changsha 410083, China (e-mail: xuxiaolei@csu.edu.cn; cjw1997@csu.edu.cn).

Hua Deng and Yi Zhang are with the State Key Laboratory of High Performance Complex Manufacturing, School of Mechanical Engineering, Central South University, Changsha 410083, China (e-mail: hdeng@csu.edu.cn; zhangyicsu@csu.edu.cn).

Digital Object Identifier 10.1109/TNSRE.2022.3214866

be well represented by Hill-type models [7], [16], [18]. On the other hand, the Huxley-type muscle model with more detailed approximation of physiological process is rarely chosen because of more computational resources to solve the nonlinear partial differential equation, when time consumption is more concerned [19], [20]. Thus, obtaining a low dimensional Huxley-type muscle model as well as balancing the model complexity and accuracy are necessary for the efficient and stable implementation of this model.

Huxley model can include some important characteristics of skeletal muscle under the dynamic contraction [21], [22]. One of the main assumptions is that actin–myosin binding reactions obey first-order kinetics, which are expressed by a partial differential equation. The nonlinear partial differential equation with time and space dependence belongs to an infinite-dimensional system and it is thus difficult to analyze and solve the equation in real applications. In early work, Zahalak [23] proposed an analytical solution for the distribution of attached cross bridges using the method of characteristics. However, due to the low computational efficiency of this method, this solution is considered unacceptable for solving practical problems. Later, various complicated approximate models were proposed for this theory [24], [25] but only have numerical solutions. Thus, Huxley-type model prefers to be applied in computational simulations [24], [25], [26] instead of real-time force estimations despite its accurate reflection of delicate muscle movements.

This study aimed to solve the differential equation of the Huxley-type skeletal muscle contraction model and use the low-dimensional musculoskeletal model driven by sEMG signals to obtain more accurate and practical grasping force estimates. First, in Sections II and III, the time and space components of the Huxley-type model are separated using a spectral method, and the balanced truncation method is used to further reduce the model dimensionality, forming a very low-dimensional skeletal muscle dynamic model. Next, Section IV describes the multi-channel EMG signal grabbing force extraction method based on the Kalman filter, which achieved more accurate and low-latency grabbing force signal extraction. The particle swarm optimization method is then used to identify the model parameters. Finally, to verify the effectiveness of this method, a total of 150 experiments were carried out on different 10 days during one month with an interval of 2-14 days by three participants, and the results are presented in Section V. The advantages and limitations of this method are discussed in Section VI.

II. Huxley-Type Musculoskeletal Model

In the Huxley-type model shown in Fig. 1, the sarcomere is the basic contractile unit of the muscle fiber, which is composed of two main filaments—actin and myosin. After receiving the action potential, the calcium ion concentration of the sarcomere will increase, prompting the actin and myosin binding to form cross-bridges. Meanwhile, adenosine triphosphate (ATP) will hydrolyze to adenosine diphosphate (ADP) and phosphoric acid (Pi), causing the cross-bridges to swing. It is a cycle of repetitive events that causes actin and myosin myofilaments to slide over each other, contracting the sarcomere and generating tension in the muscle.

According to Huxley's skeletal muscle contraction model [26], [27], the actin–myosin binding reaction obeys

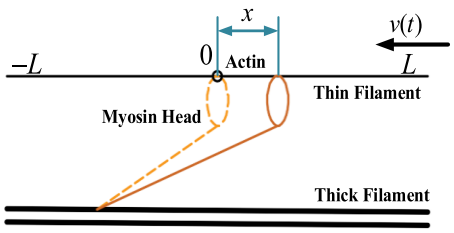

Fig. 1. Huxley-type actin–myosin binding reaction model in the sarcomere.

the following kinetics equation:

$$\frac{\partial p(x,t)}{\partial t} - \upsilon(t)\frac{\partial p(x,t)}{\partial x} = r(t)f(x,t)[1-p(x,t)] - g(x,t)p(x,t), \tag{1}$$

where $\upsilon(t)$ represents the rate of myofilament slippage, $x = x_r/h$ represents the normalized value of $x_r$with the scaling factor h, x_r is the distance between the cross-bridge binding site and the equilibrium position, $p(x,t)$ is the distribution function of the number of cross-bridge binding sites, and the independent variables are the time t and the position x. $f(x,t)$ represents the reverse (separation) rate function, $g(x,t)$ represents the forward (combination) rate function, and $r(t)$ represents the activation function of the muscle.

Once $p(x,t)$ is determined, the moments of the distribution can be used to calculate various macroscopic variables of interest. It is assumed that the force–displacement relationship of the cross-bridge is described by a linear spring constant k and the muscle is fully activated. The force is calculated as follows [26]:

$$F(t) = \frac{Qm\eta sh^2}{2l}\int_{-L}^{L} xp(x,t)dx, \tag{2}$$

where Q is the cross-sectional areas of the muscle, m is the number of cross-bridges per unit volume, η is a linear spring constant of cross-bridges, s is the length of the sarcomere, l represents the distance between successive actin binding sites, and L represents the maximum value of x.

In this model, we have the following three assumptions:

Authors should consider the following points:

1) When muscle fatigue and other physiological changes are not considered in a short period, the rate functions $f(x,t)$ and $g(x,t)$ are generally defined as functions of x but not of t. In other words, it is assumed that at any two moments in a short period, when the number of cross-bridges, the myoelectricity activation strength, and the sliding displacement of the myofilaments are the same, the changes in the distribution function of the cross-bridges are also the same. The following rate function was used in the simulation process [28]:

$$f(x) = 3\lambda e^{(-x^2/2)}, \quad g(x) = \lambda(0.15 + e^{(-1.5x)}), \tag{3}$$

2) The EMG signal controls the binding ability of the transverse bridge by regulating the concentration of calcium ions in the muscle mass, and this process involves a relatively complex chemical change [23]. However, compared to the sampling rate of the EMG signal, this process occurs extremely fast. Therefore, the normalized

EMG signal and the degree of muscle activation can be described by the function [29]:

$$r(t) = \left(e^{\gamma\,\alpha(t)} - 1\right) \Big/ \left(e^{\gamma} - 1\right), \tag{4}$$

where $\alpha(t)$ is the filtered EMG signal, whose acquisition process is described in Section IV, γ is a constant parameter of the non-linear shape factor that is allowed to vary between -3 and 0. When γ equals -3, the function is highly exponential, and when γ equals 0, the function is linear.

3) According to the biological principles of skeletal muscles, it is known that outside the range of movement of the transverse bridge in the x-direction, the binding rate of the transverse bridge is almost zero. At the same time, it is assumed that when the muscle is in a relaxed state, the combination of the cross-bridges forms an approximately normal distribution. Thus, the following boundary conditions were selected:

$$p(-L, t) = p(L, t) = 0;$$
$$p(x, 0) = \frac{p_0}{\sqrt{2\pi}\,\sigma} e^{\left(-\frac{(x-\mu)^2}{2\sigma^2}\right)}. \tag{5}$$

This biological model is based on a nonlinear partial differential equation, which belongs to an infinite-dimensional system with space and time dependence. As a result, analytical solutions are difficult to obtain. Thus, it is difficult to analyze the dynamic characteristics of the muscle force. In addition, some parameters in the model are unknown, and some biological processes have no accurate model explanation. The EMG estimation method based on Huxley's skeletal muscle model does not have a convenient and practical general model, which limits its application.

Therefore, the next step is to derive accurate and effective solutions of the partial differential equations governing the theory of muscle contraction and cross-bridges to obtain a practical prosthetic hand muscle model with easy-to-identify parameters. This means that the dimensions of the cross-bridge model need to be reduced first.

III. Muscle Model Dimensionality Reduction Based On Spectral Method and Balanced Truncation

The distributed moment method was first used to find the solution for the muscle model, and three ordinary differential equations were obtained for the first three moments. This approach evolved to encompass many different muscle types and behaviors [23], [30]. Meanwhile, a spatial approximation and a multistep Adams–Moulton method was used to solve the partial differential equation and showed a higher accuracy and efficiency [31]. However, compared to the former simplified low-dimensional result, the spatial approximation result is too complicated to be modified or made more sophisticated to model other systems.

To obtain a practical biological muscle model, the following three steps (also shown in Fig. 2) were used. First, a spectral method and the Galerkin method were applied to reduce the model dimensionality. Second, the balanced truncation method was used to further reduce the dimensionality, and a very low-dimensional skeletal muscle dynamics model was obtained. Finally, the time and space variables were integrated, and a low-dimensional muscle mechanics model was obtained based on the relationship between the muscle force and speed.

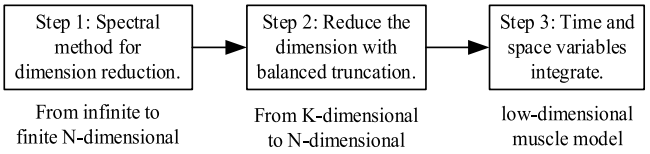

Fig. 2. Overview of dimensionality reduction steps.

A. Spectral Method for Dimension Reduction

Based on the boundary conditions given by (5), the basis function of the spectral method is chosen as follows:

$$\varphi_n(x) = \sin\left(n\pi(x + L)\big/2L\right). \tag{6}$$

According to the separation of variables method, $r(t)f(x,t)$ and $p(x,t)$ in Equation (1) can be expressed as follows:

$$r(t)f(x,t) = u(x,t) = \sum_{n=1}^{N} u_n(t)\varphi_n(x), \tag{7}$$

$$p(x,t) = \sum_{n=1}^{N} a_n(t)\varphi_n(x). \tag{8}$$

where $u_n(t)$ and $a_n(t)$ are the separated time variables.

Substituting (7) and (8) into (1) yields

$$\begin{aligned}\sum_{n=1}^{N} \dot{a}_n(t)\varphi_n(x) &= v(t)\sum_{n=1}^{N} a_n(t)\dot{\varphi}_n(x) - g(x)\sum_{n=1}^{N} a_n(t)\varphi_n(x) \\ &\quad + \sum_{n=1}^{N} u_n(t)\varphi_n(x) - r(t)f(x)\sum_{n=1}^{N} a_n(t)\varphi_n(x).\end{aligned} \tag{9}$$

Equation (9) can be written in the form of an infinite-dimensional system of differential equations:

$$\begin{aligned}0 = \dot{a}_n(t)\varphi_n(x) - v(t)a_n(t)\dot{\varphi}_n(x) + g(x)a_n(t)\varphi_n(x) \\ - u_n(t)\varphi_n(x) + r(t)f(x)a_n(t)\varphi_n(x).\end{aligned} \tag{10}$$

where $n = 0, 1, 2, \cdots, +\infty$

The nonlinear Galerkin method is used to project onto each orthogonal basis in space [32]:

$$\begin{aligned}0 = \dot{a}_n(t)\int_{-L}^{L}\sum_{m=1}^{M}\varphi_m(x)\varphi_n(x)dx - v(t)a_n(t) \\ \times \int_{-L}^{L}\sum_{m=1}^{M}\dot{\varphi}_m(x)\varphi_n(x)dx \\ + a_n(t)\int_{-L}^{L}\sum_{m=1}^{M} g(x)\varphi_m(x)\varphi_n(x)dx - u_n(t) \\ \times \int_{-L}^{L}\sum_{m=1}^{M}\varphi_m(x)\varphi_n(x)dx \\ + r(t)a_n(t)\int_{-L}^{L}\sum_{m=1}^{M} f(x)\varphi_m(x)\varphi_n(x)dx,\end{aligned} \tag{11}$$

where

$$u_n(t)\int_{-L}^{L}\sum_{m=1}^{M}\varphi_m(x)\varphi_n(x)dx$$
$$=\int_{-L}^{L}\sum_{n=1}^{N}u_n(t)\varphi_n(x)\varphi_n(x)dx$$
$$=r(t)\int_{-L}^{L}f(x)\varphi_n(x)dx. \quad (12)$$

After performing the integration in (11) and (12), the following ordinary differential equations are obtained:

$$\frac{da_n(t)}{dt}=b_n a_n(t)+u_n r(t)+[h_{Vn}v(t)+h_{Rn}r(t)]\,a_n(t), \quad (13)$$

where

$$b_n=-\frac{1}{L}\left[\int_{-L}^{L}\sum_{m=1}^{M}g(x)\sin\frac{m\pi(x+L)}{2L}\sin\frac{n\pi(x+L)}{2L}dx\right], \quad (14)$$

$$u_n=\frac{1}{L}\left[\int_{-L}^{L}f(x)\sin\frac{n\pi(x+L)}{2L}dx\right], \quad (15)$$

$$h_{Vn}=\frac{1}{L}\left[\int_{-L}^{L}\sum_{m=1}^{M}\frac{m\pi}{2L}\cos\frac{m\pi(x+L)}{2L}\sin\frac{n\pi(x+L)}{2L}dx\right], \quad (16)$$

$$h_{Rn}=-\frac{1}{L}\left[\int_{-L}^{L}\sum_{m=1}^{M}f(x)\sin\frac{m\pi(x+L)}{2L}\sin\frac{n\pi(x+L)}{2L}dx\right]. \quad (17)$$

Based on the frequency of the basis function, the system can be divided into fast and slow systems. After removing the fast systems ($N=8$ and $M=15$, for example), the infinite-dimensional ordinary differential equation system specified by (8) and (13) can be simplified to a finite set of ordinary differential equations, which can be rewritten in the following general form:

$$\dot{a}(t)=Aa(t)+Br(t)+H(a(t),r(t))$$
$$y(t)=Ca(t). \quad (18)$$

Although the cross-bridge model contains a first derivative evaluated over a space of partial differential equations, its dimension is still relatively high.

B. Dimension Reduction With Balanced Truncation

A lower-dimensional linear time invariant system can be obtained through a linear transformation with the balanced truncation method. Suppose $a(t)=R^{-1}\tilde{a}(t)$, where R is the basic functional transformation matrix. To remove the nonlinear part of (18), let $v(t)=v_{max}$ and $r(t)=r_{max}$, yielding the following:

$$\dot{\tilde{a}}(t)=R(A+h_{Vn}v_{\max}+h_{Rn}r_{\max})R^{-1}\tilde{a}(t)+RBr(t)$$
$$y(t)=CR^{-1}\tilde{a}(t). \quad (19)$$

Due to the symmetry of the observability and controllability matrix, the SVD (Singular Value Decomposition) of the square decomposition product and the transformation matrix R can be obtained by balanced truncation with the first k columns of the matrix, $VU\Sigma^{-1/2}$. After replacing v_{max} and r_{max} with the nonlinear terms $v(t)$ and $r(t)$, respectively, the infinite-dimensional cross-bridge models can be approximated as a K-dimensional model, which can be rewritten as follows:

$$\dot{\tilde{a}}(t)=R[A+h_{Vn}v(t)+h_{Rn}r(t)]R^{-1}\tilde{a}(t)+RBr(t)$$
$$y(t)=CR^{-1}\tilde{a}(t). \quad (20)$$

To verify the effectiveness of this method, the reduced-dimensionality models presented above (N = 8, K = 2 and 3) were numerically solved and compared by obtaining the finite element solution of (1)–(5), which were discretized in variable x. The muscle velocity $v(t)$ and EMG signal $\alpha(t)$ were specified during the numerical computation.

Fig. 3 shows the steady-state error of the dimensionality reduction model with constant $\alpha(t)$ input when N = 8, K = 3, and K = 2. The steady-state was relatively large when K = 2 compared to the finite element solution. In contrast, the steady-state error of the balanced truncation result with K = 3 and the spatial approximation method with N = 8 was sufficiently small and more acceptable.

Thus, to obtain a Huxley-type muscle model with a lower dimensionality and higher accuracy, the dimensionality reduction model (K = 3) was selected. Fig. 4 shows the model's dynamic response when K = 3.

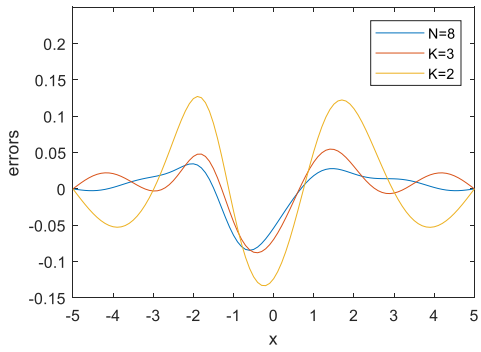

Fig. 3. Steady-state error of the dimensionality reduction model (N = 8, K = 3, and K =2) compared with the finite element solution, with the constant input $\alpha(t)=0.8$.

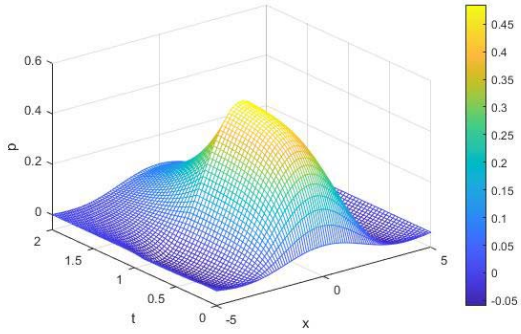

Fig. 4. Simulation result of the 3-dimensionality model with initial value ($p_0=0.1, \mu=0, \sigma=1$), and with activation input $\alpha(t)=0.8$ when $t\in[0,1]$, $\alpha(t)=0$ when $t\in[1,2]$.

C. Electromyography (EMG)-Driven Huxley-Type Musculoskeletal Force Model

In applications, it is difficult to directly measure the speed of muscle contraction. Therefore, a simple inversely proportional relationship was used to estimate the speed based on the muscle strength [21]:

$$(F + F_a)(v(t) + v_b) = (F_0 + F_a)v_b. \tag{21}$$

This can be rewritten as follows:

$$v(t) = v_b F_0 \big/ (F_a + F(t)) - v_b. \tag{22}$$

Before dimensionality reduction, it is difficult to obtain an analytical solution of Equation (1). After using the balanced truncation method with K = 3,

$$p(x,t) = \sum_{k=1}^{3} \tilde{a}_k(t)\psi_k(x), \tag{23}$$

$$\psi_k(x) = \sum_{j=1}^{N} R_{jk}\varphi_j(x). \tag{24}$$

where R_{jk} denotes the j row and k column of basic functional transformation matrix R. $\varphi_j(x)$ denotes the jth basis function.

Substituting (21), (22), (23), (24), and (2) into (1) yields:

$$\dot{\tilde{a}}_k(t) = \tilde{A}_k(t)\tilde{a}_k(t) + \tilde{B}_k r(t), \quad k = 1, 2, 3, \tag{25}$$

$$F(t) = \sum_{k=1}^{3} \tilde{a}_k(t) \frac{Qm\eta sh^2}{2l} \int_{-L}^{L} x\psi_k(x)dx, \tag{26}$$

where

$$\tilde{A}_k(t) = h_{Rk}r(t) + h_{Vk}(v_a(t) - v_b) + b, \quad k = 1, 2, 3, \tag{27}$$

$$v_a(t) = \frac{v_b F_0}{F_a + \sum_{k=1}^{3} \tilde{a}_k(t) \frac{Qm\eta sh^2}{2l} \int_{-L}^{L} x\psi_k(x)dx}, \tag{28}$$

Notice that the following terms can be directly obtained by integration:

$$C_k = \frac{Qm\eta sh^2}{2l} \int_{-L}^{L} x\psi_k(x)dx. \tag{29}$$

The EMG-driven Huxley-type musculoskeletal force model can be obtained as follows:

$$\dot{\tilde{a}}_k(t) = \tilde{A}_k(t)\tilde{a}_k(t) + \tilde{B}_k r(t), \quad k = 1, 2, 3, \tag{30}$$

$$\tilde{A}_k(t) = h_{Rk}r(t) + v_b h_{Vk}\left(\frac{F_0}{F_a + F(t)} - 1\right) + b, \quad k = 1, 2, 3, \tag{31}$$

$$F(t) = \sum_{k=1}^{3} C_k \tilde{a}_k(t). \tag{32}$$

The following variables exist in the model:

C_0, C_1, C_2 are related to the muscle force $F(t)$; v_b, F_0, F_a are related to the muscle speed $v(t)$; $b, h_{R1}, h_{R2}, h_{R3}$, h_{V1}, h_{V2}, h_{V3} are related to the state function $a(t)$; B_0, B_1, B_2 are related to the input EMG signal $r(t)$.

The calculated sequences are (31), (30), (32), and the initial values at $t = 0$ of the equations are given as follows:

$$F(0) = 0, \tag{33}$$

$$\tilde{a}_k(0) = 0, \quad k = 1, 2, 3. \tag{34}$$

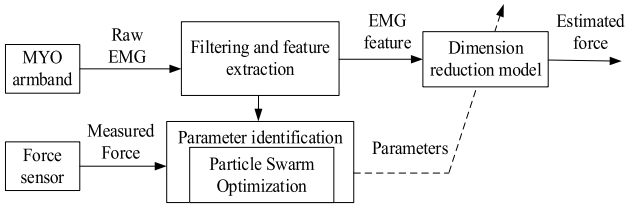

Fig. 5. Force estimation method based on dimensionality reduction model.

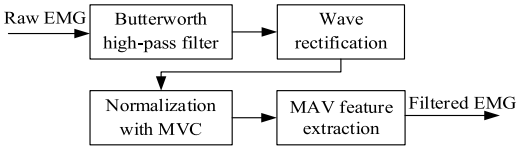

Fig. 6. Force estimation method based on reduced-dimensionality model.

IV. Parameter Identification and Grasping Force Estimation Method Based on Reduced-Dimensionality Huxley-Type Skeletal Muscle Model

After completing the dimensionality reduction of the skeletal muscle biological model, there are still many unknown parameters in the model, and most of these parameters are related to the biological characteristics of the human body. Therefore, these parameters need to be identified before the grasping force estimation. To obtain accuracy and stable force estimation results, the estimation method is proposed as shown in Fig. 5.

A. Filtering and Feature Extraction of Raw EMG Signal

The MYO armband used in this study could obtain the original EMG signal on eight electrodes at a sampling frequency of 200 Hz and send it to the computer via Bluetooth. However, the original EMG signal contained a considerable amount of noise, so it was necessary to filter the signal first. The general commonly used filtering steps are as follows [2], [3], [4], [5]. First, the 4th-order Butterworth high-pass filter (30Hz) were applied to remove motion artifacts, and then the wave rectification and normalization with the peak of maximum voluntary contraction (MVC) were used for EMG processing. Finally, the mean absolute value (MAV) feature of EMG signal was used as the input of reduced-dimensionality model.

During MAV feature extraction require the extraction of a smooth envelope of the EMG signal. This is usually achieved by low-pass filtering, which introduces time lags due to phase distortion. Offline, this error is easily compensated by zero-phase filtering, however, not suitable for real-time state-space based myoelectric control. Thus, a standard Kalman filter was used to extraction the MAV feature of EMG signal [33], as shown in Fig. 6.

To filter the noise of the ith channel's EMG signal at time τ, the model and measurement equations are written in the following general form:

$$\begin{aligned} \alpha_{\tau+1}^{i} &= \alpha_{\tau}^{i} + \Delta\alpha_{\tau}^{i} + G_\tau w_\tau \\ z_{\tau}^{i} &= \alpha_{\tau}^{i} + v_\tau, \end{aligned} \tag{35}$$

where $x_0 \sim (\bar{x}_0, P_{x0})$, $w_\tau \sim (0, \mathrm{Q}_\tau)$, $v_\tau \sim (0, R_\tau)$.

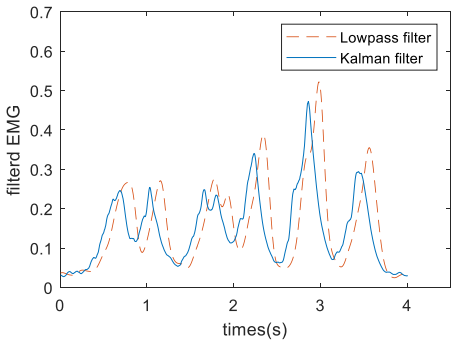

Fig. 7. Result of the EMG processing based on the Kalman filter and low-pass filter during MAV feature extraction.

z_τ^i is the rectified EMG signal at time τ of channel i, w_τ is the process noise, and v_τ is the measurement noise.

With $x_\tau = \left[\alpha_\tau^1, \alpha_\tau^2, \ldots, \alpha_\tau^i, \Delta\alpha_\tau^1, \Delta\alpha_\tau^2, \ldots, \Delta\alpha_\tau^i\right]$, the filtered α_τ^i can be acquired from the following updating equation [27]:

$$P_0 = P_{x0}, \quad \hat{x}_0 = \bar{x}_0, \tag{36}$$

The status updating equation is as follows:

$$\begin{aligned} P_{\tau+1}^- &= A_\tau P_\tau A_\tau^T + G_\tau Q_\tau G_\tau^T \\ \hat{x}_{\tau+1} &= \hat{x}_\tau, \end{aligned} \tag{37}$$

The estimated value updating equation is as follows:

$$\hat{x}_{\tau+1} = \hat{x}_{\tau+1}^- + L_{\tau+1}[z_{\tau+1} - H_{\tau+1}\hat{x}_{\tau+1}^-], \tag{38}$$

The error covariance updating equation is as follows:

$$P_{\tau+1} = (I - L_{\tau+1}H_{\tau+1})P_{\tau+1}^-, \tag{39}$$

The Kalman gain updating equation is as follows:

$$L_{\tau+1} = P_{\tau+1}^- H_{\tau+1}^T (H_{\tau+1} P_{\tau+1}^- H_{\tau+1}^T + R_{\tau+1})^{-1}. \tag{40}$$

The results of the EMG signal extraction using this method were compared with the low-pass filter with a cut-off frequency of 2 Hz and the parameters Q and R of the Kalman filter are set to 0.01 and 2.6 respectively.

Fig. 7 shows that the EMG signal extraction method based on the Kalman filter could obtain more real-time signals. The ordinary low-pass filter had a similar processing effect, but it had a delay of more than 100 ms. Therefore, the EMG signal extraction method based on the Kalman filter was chosen for the grasping force estimation and control.

B. Parameter Identification With Particle Swarm Optimization Algorithm

Since there are some unknown parameters in the model, and most of them have non-linear relationships, a particle swarm optimization algorithm was used to tune and optimize the model parameters. The calculation steps were as follows:

1) The input vector containing the variables defined above is set as follows:

$$\begin{aligned} Parameter = [&\gamma, b, B_1, B_2, B_3, C_1, C_2, C_3, h_{R1}, \\ &h_{R2}, h_{R3}, h_{V1}, h_{V2}, h_{V3}, F_0, F_a]. \end{aligned} \tag{41}$$

2) The following objective function was used to minimize the error between the estimated grasping force F_p and the actual grasping force F_t:

$$J = \sqrt{\sum_{\tau=1}^{T} \left[F_p(\alpha_\tau, Paramter) - F_t(\alpha_\tau, Paramter)\right]^2}. \tag{42}$$

3) The initial values and ranges were set as follows:
$\gamma \in [-3, 0]$, according to (4);
$b \in [-2, 0]$, according to (14);
$B_1 \in [0, 1]$, $B_2 \in [-2, 0]$, $B3 \in [-1, 0]$, according to (15);
$h_{V1}, h_{V2}, h_{V3} \in [-1, 0]$, according to (16);
$h_{R1}, h_{R2}, h_{R3} \in [-3, 0]$, according to (17);
$C_1, C_2, C_3 \in [-20, 20]$, according to (29);
and the range of forces
$F_0 \in [0, 3]$, $F_a \in [0, 10]$, according a previous publication [34].
4) Initial particles and velocities were randomly generated in the interval near the initial value with $v \in [0.5, -0.5]$, and the fitness and optimal particles were calculated.
5) The iterative calculation was performed with the following steps:
Particle speed updating, particle population updating, fitness updating, selection of the best selection of the best particle, and repeating of these steps until $J \leq J_{\min}$.

This process was performed offline since there were many parameters that needed to be identified, and to ensure the accuracy of the model, the iteration process (5) will be repeated more than 1000 times in practice. Fortunately, unless the model was completely invalidated with significant physiological changes, this process would only need to be performed once a new person participated in the experiment.

V. Grasping Force Estimation Experiment Design and Verification

To verify the accuracy and long-term stability of the skeletal muscle reduced-dimensionality model proposed in this article, a total of 150 experiments were performed on different 10 days during one month with an interval of 2-14 days by three participants. The raw data of the surface EMG signal was collected by the MYO armband from Thalmic Labs and sent to the computer wirelessly. When using the model-based force estimation method, the cutoff frequency generally does not exceed 200Hz [4], [16]. Therefore, the 200Hz sampling rate was used for this method.

The grasping force data was obtained by designing a spherical grasped sample, which contained a built-in JHBM-H3 plane force sensor that could measure a grasping force of 0–50 N. As shown in Fig. 8 and Fig. 9, the spherical grasped sample consists of two plastic hemispheres and is connected by a force sensor and a few of screws in the middle. The grasping force signal was collected by an NI USB-6211 multifunction input/output device, and the sampling frequency was the same as that of the armband.

A. Offline Full-Parameter Identification Experiment Based on Particle Swarm Optimization Algorithm

The parameters were identified and optimized using the particle swarm optimization algorithm with the experimental data.

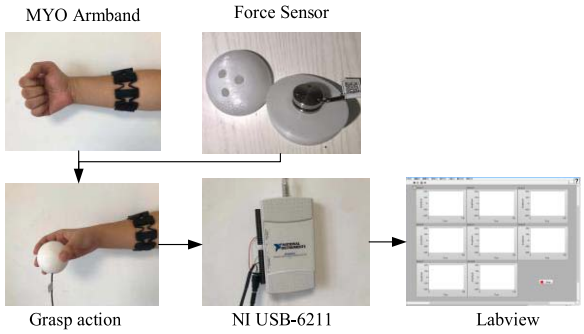

Fig. 8. Grasping force estimation experimental process and equipment.

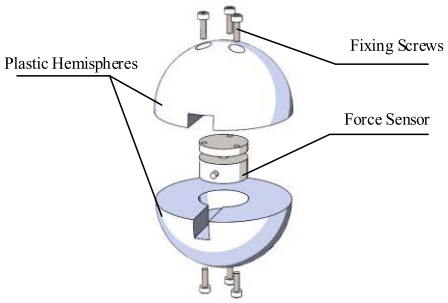

Fig. 9. Structure of the spherical grasped sample with force sensor.

Due to a large amount of identification data and parameters, this process must generally be performed offline. The first part of the experimental process was as follows:

1) Alcohol was used to wipe the location where the armband was worn to ensure good contact between the armband and the skin. The armband was then put on the arm close to the elbow joint, and the sampling procedure was started.
2) The spherical sensor was held, and then the arm muscles were relaxed until the amplitudes of the EMG signal fluctuations were small and stable.
3) The signal acquisition was started. During the experiment, a grasping force was applied to the grasped sample. Five kinds of grasping tasks were performed: linear increase (5 s), step increase with three stages (5 s), intermittent increase and decrease (5 s), continuous increase and decrease (5 s), and rapid increase and decrease (5 s).
4) The duration of one set of experiments was 25–30 s, and the parameters were identified and optimized using the particle swarm optimization algorithm with the experimental data.

The grasping force estimation performance was evaluated by the mean absolute error (MAE), mean square error (MSE), coefficient of determination (R^2) and correlation coefficient (CC), defined as follows:

$$MAE = \frac{1}{N}\sum_{i}^{N}|x_i - y_i|, \tag{43}$$

$$MSE = \frac{1}{N}\sum_{i}^{N}(x_i - y_i)^2, \tag{44}$$

TABLE I
EVALUATION RESULTS OF PARAMETER IDENTIFICATION

No.	Date	Gender	Age	Largest estimate force	MAE	MSE	R^2
1	Day 1	male	29	41.67	1.85	6.77	94.50%
2	Day 1	male	27	31.30	1.78	6.70	94.31%
3	Day 1	female	25	21.34	1.11	2.62	94.51%

TABLE II
THE CC VALUE OF PARAMETER IDENTIFICATION WITH FIVE KINDS OF GRASPING EXPERIMENTS

No.	Date	Gender	Task1	Task2	Task3	Task4	Task5
1	Day 1	male	0.9770	0.9732	0.9860	0.9560	0.9750
2	Day 1	male	0.9881	0.9821	0.9755	0.9637	0.9702
3	Day 1	female	0.9758	0.9795	0.9724	0.9804	0.9573

$$R^2 = 1 - \frac{1}{N}\frac{\sum_{i}^{N}(x_i - y_i)^2}{\sum_{i}^{N}(x_i - \bar{x})^2}, \tag{45}$$

$$CC = \frac{\sum_{i=1}^{N}(x_i - \bar{x})(y_i - \bar{y})}{\sqrt{\sum_{i=1}^{N}(x_i - \bar{x})^2 \sum_{i=1}^{N}(y_i - \bar{y})^2}}. \tag{46}$$

where x_i represents the measured forces, y_i represents the estimated forces, $\bar{x}$ represents the average of the measured forces, and N is the number of samples.

For each participant, the method uses 30s of valid data collected on the first day for parameter identification, about 6000 sample data. The offline identification results are shown in Table I, Table II and Fig. 10. Results show that the identification results are accurate for different grasping tasks. The CC value is high enough and change between 0.9573-0.9881.

B. Huxley-Type Musculoskeletal-Model-Based Grasping Force Estimation Experiment

In this part of the experiment, parameter identification was not performed. The purpose of the experiment was mainly to verify the stability and accuracy of the model.

Using the model given by (30)–(32), the grasping force predicted by the model could be compared with the measured grasping force. The following steps were involved in the experimental procedure:

1. The armband was worn again after a period of time, and steps 1–3 of the first part experimental process were repeated. At the same time, the grasping forces were estimated in LABVIEW with the collected signals by the method proposed in Section IV.
2. The duration of one set of experiments was 25 s, and a total of ten sets of experiments were carried out.

To verify the long-term validity of the model, the above experimental procedure was repeated 150 times during a month with an interval of 2-14 days by three participants. The experimental results of the grasping force estimation are shown in Fig. 11.

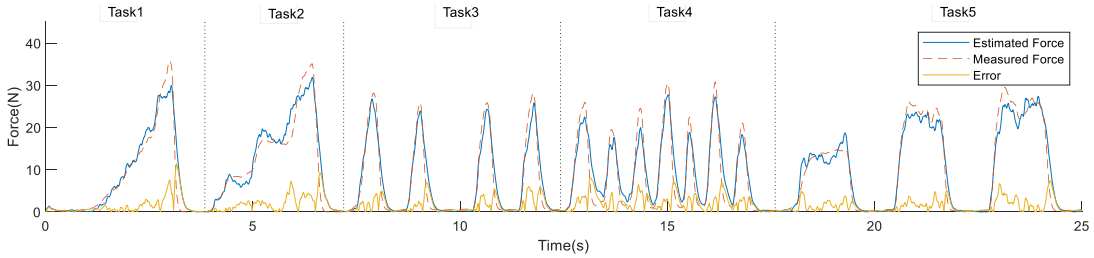

Fig. 10. Parameter identification results with particle swarm optimization algorithm on day 1 with five kinds of grasping tasks.

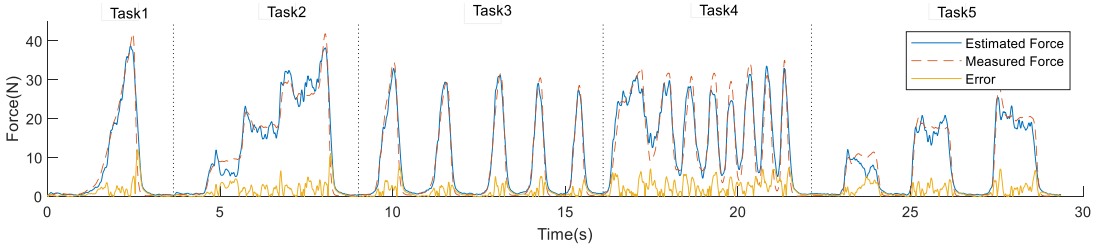

Fig. 11. Grasping force estimation result based on reduced Huxley-type musculoskeletal model on day 31 with five kinds of grasping tasks.

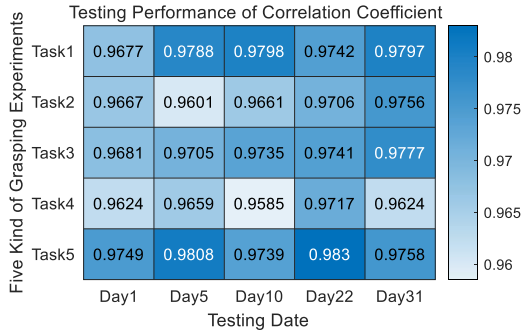

Fig. 12. The testing performance of CC values for the first participant with five kinds of grasping force estimated tasks on different five days.

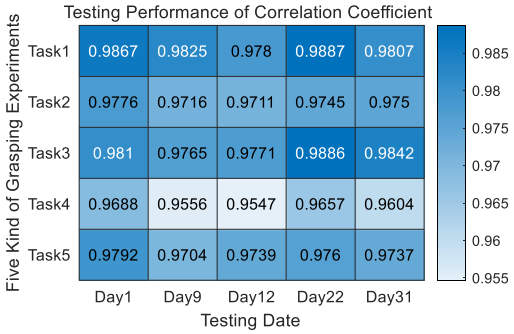

Fig. 13. The testing performance of CC values for the second participant with five kinds of grasping force estimated tasks on different five days.

TABLE III
AVERAGE EVALUATION RESULTS OF THE FIRST PARTICIPANT WITH THE FORCE ESTIMATED EXPERIMENTS

No.	Data	Average largest test force	Average testing MAE	Average testing MSE	Average testing R^2
1	Day 1	38.11	1.89	8.37	92.65%
2	Day 5	34.48	1.50	5.20	93.18%
3	Day 10	34.60	1.74	6.96	92.68%
4	Day 22	37.69	1.95	8.28	92.94%
5	Day 31	38.11	1.80	7.51	93.60%

The five kinds of grasping tasks results of the first participant in a month are shown in Fig. 12. The minimum CC value appears at task4 on the 10th day is 0.9585, and the maximum CC value appears at task5 on the 22nd day is 0.983. Across all days, task5 has the highest average accuracy of 0.9777 and task4 has the lowest average accuracy of 0.9642. In terms of daily performance, the daily CC average values are stable changing from 0.968 to 0.9742.

The overall evaluation results of the first participant in a month are shown in Table III. For participant 1, the average maximum grasping force was 36.598 N, the average MAE was 1.776, the average MSE was 7.264, and the average R^2 was 93.010%. According to the value of the maximum grasping force amplitude, the model had high accuracy in the range of grasping forces of 0–38 N.

The five kinds of grasping tasks results of the second participant in a month are shown in Fig. 13. The minimum CC value appears at task4 on the 10th day is 0.9547, and the maximum CC value appears at task1 on the 22nd day is 0.9887.

Across all days, task1 has the highest average accuracy of 0.9833 and task4 has the lowest average accuracy of 0.9611. In terms of daily performance, the daily CC average values are stable changing from 0.971 to 0.9787.

The evaluation results of the second participant over a month are shown in Table IV. For participant 2, the average maximum grasping force was 32.276 N, the average MAE was 1.722, the average MSE was 6.810, and the average R^2 was 93.180%. According to the value of the maximum grasping force amplitude, the model had high accuracy in the range of grasping forces of 0–34 N. When the grasping force reached 36 N, the accuracy decreased, but it was still above 90%.

The five kinds of grasping tasks results of the first participant in a month are shown in Fig. 14. The minimum CC value

TABLE IV
AVERAGE EVALUATION RESULTS OF THE SECOND PARTICIPANT WITH THE FORCE ESTIMATION EXPERIMENTS

No.	Data	Average largest test force	Average testing MAE	Average testing MSE	Average testing R^2
1	Day 1	29.97	1.60	5.37	94.55%
2	Day 9	34.39	1.63	6.24	93.00%
3	Day 12	28.17	1.51	5.43	92.24%
4	Day 22	32.49	1.65	6.33	93.98%
5	Day 31	36.39	2.22	10.68	92.13%

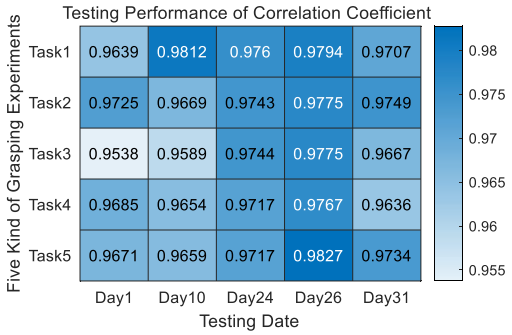

Fig. 14. The testing performance of CC values for the third participant with five kinds of grasping force estimated tasks on different five days.

TABLE V
AVERAGE EVALUATION RESULTS OF THE THIRD PARTICIPANT WITH THE FORCE ESTIMATION EXPERIMENTS

No.	Data	Average largest test force	Average testing MAE	Average testing MSE	Average testing R^2
1	Day 1	25.37	1.70	5.61	91.66%
2	Day 10	20.80	1.17	3.07	92.84%
3	Day 24	26.62	1.73	6.08	91.37%
4	Day 26	32.46	1.51	5.45	93.91%
5	Day 31	30.56	1.63	5.66	93.99%

appears at task3 on the 1th day is 0.9538, and the maximum CC value appears at task5 on the 22nd day is 0.9827. Across all days, task1 has the highest average accuracy of 0.9742 and task3 has the lowest average accuracy of 0.9663. In terms of daily performance, the daily CC average values are stable changing from 0.9652 to 0.9788.

The evaluation results of the third participant over a month are shown in Table V. For participant 3, the average maximum grasping force was 27.162 N, the average MAE was 1.548, the average MSE was 5.174, and the average R^2 was 92.754%. The grasping force of the test participant was relatively small overall, but the model also had a high accuracy within 0–32 N.

In a conclusion, task1 has a high accuracy, with an overall average of 0.9779, and task4 has the lowest accuracy, with an overall average of 0.9648 which is accuracy enough. In addition, with the longest interval of same tasks for each participant, the accuracy just decreased by 1.5%, 2.24% and 1.87%, respectively. The MAE and MSE values were relatively small, with average mean values of 1.682 and 6.416, respectively, and the recognition accuracy of the three participants exceeded 90%. The grip strengths of the three participants were different, and the recognition range of the grip strength could cover the normal range of grasping force. In addition, after the model was trained on the first day, there was no significant decline in the estimation during the test over the next month. This means that long-term stability was obtained.

Compared with the continuous force estimation realized by support vector regression (SVR) and multi-modal feature combination proposed by Mao et al [15], the proposed grasping force estimation method can improve the performance of the CC value by 1.93% and required less training set. On the other hand, compared with a 5-day repeatability experiment showed a 4.1% decrease of classification accuracy per day [35], this method has no significant decline during 30 days with the largest variation of 2.69% under same task. In general, the proposed method with dimensionality reduction model showed more accuracy and stable continuous force estimation performance compared with previous studies.

VI. DISCUSSION

The Huxley-type musculoskeletal muscle model is based on a nonlinear partial differential equation, which belongs to an infinite-dimensional system with space and time dependence. These characteristics make the differential equation difficult to solve, which limits the application of the model. To solve this problem, the spectral method and the balanced truncation method were used to reduce the dimensionality of the model, and theory was involved for the parameter identification, realizing accurate and stable grasping force estimates finally. The innovation and advantages of this method are as follows:

(1) An efficient force estimation method based on sEMG signals was obtained by reducing the dimensionality of the Huxley-type muscle model. As shown in the experiments, after being trained on the first day, the accuracy of the model was ensured for the next month.
(2) Due to the biological principles of this model and the physical meanings of the parameters, it is convenient to modify the model to improve the accuracy and avoid overfitting by parameter correction.
(3) By using the Kalman filtering, the real-time applicability and practicality of the model were further improved, which made it more suitable for real-time force control and muscle state monitoring based on electromyography, with wide application prospects.

In addition, problems and future improvements of this method are described as follows:

(1) The influence of the shape of the object, the kinematics, and the dynamics of the skeleton were ignored in the model. Therefore, to achieve a more accurate estimation, the kinematics and dynamics parameters of the participants' hands need to be measured and tuned. However, for the application of muscle prosthetics, these characteristics can be replaced by the parameters of the prosthesis, which are easy to obtain.
(2) A more general skeletal muscle model is used in this method, which not only ensures the stability and accuracy of the force estimation but also inherits the model's errors. To further improve the accuracy, a more complex muscle model can be introduced that also requires re-balancing between the model complexity and accuracy. However, the accuracy and stability of the model are sufficient for most applications based on myoelectricity.

As a result, this method has good application prospects for myoelectric force control and provides a potential method for human grasping force estimation.

VII. Conclusion

In this study, a reduced Huxley-type musculoskeletal model, featuring with low complexity, was proposed to estimate the grasping force, which achieves high recognition stability and real-time estimation. Different types of experiments were carried out to verify the effectiveness and stability of the method proposed. The experimental results showed that the estimated force based on the model after dimensionality reduction matched the actual measured grasping force closely, with a relatively stable estimation result after a long-time test. Despite owning accurate estimation results and reduced computational cost, the model after dimensionality reduction is still a third-order ordinary differential equation with a number of undetermined parameters. In the future, we will improve this force estimation method by further reduce the model dimensionality and decrease the undetermined parameters, making it more suitable for practical applications.

References

[1] A. W. Franzke, M. B. Kristoffersen, V. Jayaram, C. K. van der Sluis, A. Murgia, and R. M. Bongers, "Exploring the relationship between EMG feature space characteristics and control performance in machine learning myoelectric control," *IEEE Trans. Neural Syst. Rehabil. Eng.*, vol. 29, pp. 21–30, 2021.

[2] I. J. R. Martinez, A. Mannini, F. Clemente, and C. Cipriani, "Online grasp force estimation from the transient EMG," *IEEE Trans. Neural Syst. Rehabil. Eng.*, vol. 28, no. 10, pp. 2333–2341, Oct. 2020.

[3] C. Zeng, C. Yang, H. Cheng, Y. Li, and S.-L. Dai, "Simultaneously encoding movement and sEMG-based stiffness for robotic skill learning," *IEEE Trans. Ind. Informat.*, vol. 17, no. 2, pp. 1244–1252, Feb. 2021.

[4] Z. Zhu et al., "EMG-force and EMG-target models during force-varying bilateral hand-wrist contraction in able-bodied and limb-absent subjects," *IEEE Trans. Neural Syst. Rehabil. Eng.*, vol. 28, no. 12, pp. 3040–3050, Dec. 2020.

[5] H. Xu, D. Zhang, J. C. Huegel, W. Xu, and X. Zhu, "Effects of different tactile feedback on myoelectric closed-loop control for grasping based on electrotactile stimulation," *IEEE Trans. Neural Syst. Rehabil. Eng.*, vol. 24, no. 8, pp. 827–836, Aug. 2016.

[6] Y. Liu, Z. Li, H. Liu, Z. Kan, and B. Xu, "Bioinspired embodiment for intelligent sensing and dexterity in fine manipulation: A survey," *IEEE Trans. Ind. Informat.*, vol. 16, no. 7, pp. 4308–4321, Jul. 2020.

[7] S. Pancholi and A. M. Joshi, "Improved classification scheme using fused wavelet packet transform based features for intelligent myoelectric prostheses," *IEEE Trans. Ind. Electron.*, vol. 67, no. 10, pp. 8517–8525, Oct. 2020.

[8] G. K. Patel, C. Castellini, J. M. Hahne, D. Farina, and S. Dosen, "A classification method for myoelectric control of hand prostheses inspired by muscle coordination," *IEEE Trans. Neural Syst. Rehabil. Eng.*, vol. 26, no. 9, pp. 1745–1755, Sep. 2018.

[9] A. Hazarika, P. Barman, C. Talukdar, L. Dutta, A. Subasi, and M. Bhuyan, "Real-time implementation of a multidomain feature fusion model using inherently available large sensor data," *IEEE Trans. Ind. Informat.*, vol. 15, no. 12, pp. 6231–6239, Dec. 2019.

[10] J. He, X. Sheng, X. Zhu, C. Jiang, and N. Jiang, "Spatial information enhances myoelectric control performance with only two channels," *IEEE Trans. Ind. Informat.*, vol. 15, no. 2, pp. 1226–1233, Feb. 2019.

[11] E. D. Engeberg, "A physiological basis for control of a prosthetic hand," *Biomed. Signal Process. Control*, vol. 8, no. 1, pp. 6–15, Jan. 2013.

[12] K. Wang, Y. Huang, and X. Zhang, "Estimation of handgrip force from nonlinear SEMG-force relationship during dynamic contraction tasks," in *Proc. IEEE Int. Conf. Robot. Biomimetics (ROBIO)*, Dec. 2017, pp. 412–417.

[13] R. Ma, L. Zhang, G. Li, D. Jiang, S. Xu, and D. Chen, "Grasping force prediction based on sEMG signals," *Alexandria Eng. J.*, vol. 59, no. 3, pp. 1135–1147, Jun. 2020.

[14] Y. Fang, D. Zhou, K. Li, Z. Ju, and H. Liu, "Attribute-driven granular model for EMG-based pinch and fingertip force grand recognition," *IEEE Trans. Cybern.*, vol. 51, no. 2, pp. 789–800, Feb. 2021.

[15] H. Mao, Y. Zheng, C. Ma, K. Wu, G. Li, and P. Fang, "Simultaneous estimation of grip force and wrist angles by surface electromyography and acceleration signals," *Biomed. Signal Process. Control*, vol. 79, Jan. 2023, Art. no. 104088.

[16] W. Wang et al., "Prediction of human voluntary torques based on collaborative neuromusculoskeletal modeling and adaptive learning," *IEEE Trans. Ind. Electron.*, vol. 68, no. 6, pp. 5217–5226, Jun. 2021.

[17] Y. Zhuang, S. Yao, C. Ma, and R. Song, "Admittance control based on EMG-driven musculoskeletal model improves the human–robot synchronization," *IEEE Trans. Ind. Informat.*, vol. 15, no. 2, pp. 1211–1218, Feb. 2019.

[18] Y. Li, C. Jiang, M. Zheng, X. Wang, and R. Song, "Modeling ankle torque and stiffness induced by functional electrical stimulation," *IEEE Trans. Neural Syst. Rehabil. Eng.*, vol. 28, no. 12, pp. 3013–3021, Dec. 2020.

[19] A. J. van Soest, L. J. R. Casius, and K. K. Lemaire, "Huxley-type cross-bridge models in largeish-scale musculoskeletal models; an evaluation of computational cost," *J. Biomech.*, vol. 83, pp. 43–48, Jan. 2019.

[20] B. D. Doll, N. A. Kirsch, X. Bao, B. E. Dicianno, and N. Sharma, "Dynamic optimization of stimulation frequency to reduce isometric muscle fatigue using a modified Hill-Huxley model," *Muscle Nerve*, vol. 57, no. 4, pp. 634–641, Apr. 2018.

[21] H. Sugi and T. Ohno, "Physiological significance of the force-velocity relation in skeletal muscle and muscle fibers," *Int. J. Mol. Sci.*, vol. 20, no. 12, p. 3075, Jun. 2019.

[22] J. D. Powers, S. A. Malingen, M. Regnier, and T. L. Daniel, "The sliding filament theory since Andrew Huxley: Multiscale and multidisciplinary muscle research," *Annu. Rev. Biophys.*, vol. 50, no. 1, pp. 373–400, May 2021.

[23] G. I. Zahalak and I. Motabarzadeh, "A re-examination of calcium activation in the Huxley cross-bridge model," *J. Biomech. Eng.*, vol. 119, no. 1, pp. 20–29, Feb. 1997.

[24] G. Ma, Y. Wang, X. Zheng, X. Miao, and Q. Liang, "A trust-aware latent space mapping approach for cross-domain recommendation," *Neurocomputing*, vol. 431, pp. 100–110, Mar. 2021.

[25] A. J. Fenwick, A. M. Wood, and B. C. W. Tanner, "The spatial distribution of thin filament activation influences force development and myosin activity in computational models of muscle contraction," *Arch. Biochem. Biophys.*, vol. 703, May 2021, Art. no. 108855.

[26] C. Knupp and J. M. Squire, "Myosin cross-bridge behaviour in contracting muscle—The T_1 curve of Huxley and Simmons (1971) revisited," *Int. J. Mol. Sci.*, vol. 20, no. 19, p. 4892, Oct. 2019.

[27] F. L. Lewis, L. Xie, and D. Popa, *Optimal and Robust Estimation: With an Introduction to Stochastic Control Theory*. Boca Raton, FL, USA: CRC Press, 2017.

[28] T. L. Hill, "Theoretical formalism for the sliding filament model of contraction of striated muscle part I," *Prog. Biophys. Mol. Biol.*, vol. 28, pp. 267–340, 1974.

[29] J. R. Potvin, R. W. Norman, and S. M. McGill, "Mechanically corrected EMG for the continuous estimation of erector spinae muscle loading during repetitive lifting," *Europ. J. Appl. Physiol.*, vol. 74, nos. 1–2, pp. 32–119, 1996.

[30] G. M. Donovan, "Generalized distribution-moment approximation for kinetic theories of muscular contraction," *Math. Biosci.*, vol. 329, Nov. 2020, Art. no. 108455.

[31] J. Z. Wu, W. Herzog, and G. K. Cole, "Modeling dynamic contraction of muscle using the cross-bridge theory," *Math. Biosci.*, vol. 139, no. 1, pp. 69–78, Jan. 1997.

[32] H. Deng, H.-X. Li, and G. Chen, "Spectral-approximation-based intelligent modeling for distributed thermal processes," *IEEE Trans. Control Syst. Technol.*, vol. 13, no. 5, pp. 686–700, Sep. 2005.

[33] L. L. Menegaldo, "Real-time muscle state estimation from EMG signals during isometric contractions using Kalman filters," *Biol. Cybern.*, vol. 111, nos. 5–6, pp. 335–346, Dec. 2017.

[34] S. Jaric, "Force-velocity relationship of muscles performing multi-joint maximum performance tasks," *Int. J. Sports Med.*, vol. 36, no. 9, pp. 699–704, Mar. 2015.

[35] I. Kyranou, S. Vijayakumar, and M. S. Erden, "Causes of performance degradation in non-invasive electromyographic pattern recognition in upper limb prostheses," *Frontiers Neurorobot.*, vol. 12, p. 58, Sep. 2018.